Hindawi
Geofluids
Volume 2022, Article ID 1162357, 9 pages
https://doi.org/10.1155/2022/1162357

Research Article

Study on Energy Dissipation Characteristic of Ice-Rich Frozen Soil in SHPB Compression Tests

Ma Dongdong,[1,2,3] **Xiang Huasong**,[2] **Zhou Zhiwei**,[3] **Tan Yizhong**,[4] **and Wang Xinpeng**[2]

[1]*State Key Laboratory of Mining Response and Disaster Prevention and Control in Deep Coal Mine, Anhui University of Science and Technology, Huainan, 232001 Anhui, China*
[2]*School of Civil Engineering and Architecture, Anhui University of Science and Technology, Huainan, Anhui 232001, China*
[3]*Northwest Institute of Eco-Environment and Resources, State Key Laboratory of Frozen Soil Engineering, Chinese Academy of Sciences, Lanzhou, 730000 Gansu, China*
[4]*State Key Laboratory of Explosion Shock Prevention and Mitigation, Army Engineering University, Nanjing 210007, China*

Correspondence should be addressed to Ma Dongdong; dongdonm@126.com

Received 26 January 2022; Accepted 19 February 2022; Published 7 March 2022

Academic Editor: Mohammed Fattah

Frozen soil will inevitably bear dynamic loads (impact and blasting) in the construction process in cold regions; the investigation of dynamic energy dissipation characteristic of ice-rich frozen soil is beneficial to optimize blasting parameters and the design of underground explosion-proof structure. In this study, the dynamic impact laboratory tests were conducted for frozen sandy soil with various water contents (from 15% to 110%) and strain rates (from 450 s^{-1} to 728 s^{-1}) based on the split Hopkinson pressure bar (SHPB) system. The influences of strain rate, temperature, and water content on the energy parameters (i.e., absorption energy, reflected energy, and absorption energy rate) were systematically analyzed. Moreover, the energy dissipation characteristics of frozen sandy soil under different deformation stages were studied. Test results revealed that under impact load, the proportion of reflected energy to incident energy was the largest for frozen soil materials. Both the absorption energy and reflected energy were associated with strain rate. However, compared with the water content and temperature, the sensitivities of strain rate on the absorption energy rate were not obvious. At -10°C, the average absorption energy rate decreases from 17.6% to 14.5% when the water content increases from 15% to 37.5%, with a reduction of 18%. However, it substantially decreases to 6.9% at 45% water content, with a large-scale reduction of 61% compared with that at 15% water content. The energy dissipation parameters (i.e., absorption energy, releasable elastic strain energy, and dissipation energy) were closely associated with the water content, temperature, and strain rate.

1. Introduction

Frozen soil is a typical thermo-sensitive geotechnical engineering material, and its particularity is mainly manifested in two aspects: the temperature is below 0°C and the soil particles must be cemented by ice. Therefore, the mechanical responses of frozen soil under external loads cannot be directly depicted by conventional soil mechanics theory because of the existence of the ice phase [1–3]. In fact, a large number of infrastructural engineering projects, such as pipelines, power grids, roads, and railways, are built and operated in cold regions. As an important parameter in the safety design of an engineering construction process, numerous studies have been performed to acquire the mechanical and energy response of frozen soil to various types of loads (e.g., weight of building structure, train vibration, and blasting) [4–6]. Moreover, the effects of soil type, stress state, and temperature on its properties also have been systematically investigated [7].

The ice-rich frozen soil refers to soil with volumetric ice content greater than 25% [8]; a multitude of engineering practices indicate that traditional frozen soil mechanics theory departs when it is used in ice-rich frozen soil. Therefore, the impact of the subject has influenced diverse investigations in the static mechanics properties of ice-rich frozen soil [9–11]. Yang et al. [12] studied the relationship between

Table 1: The particle size distribution of soil.

Particle size range (mm)	0~0.075	0.075~0.3	0.3~0.6	0.6~1.0	1.0~2.0
Proportion (%)	1.22	7.17	41.15	30.05	20.41

Figure 1: The prepared ice-rich frozen sandy soil specimen.

static compressive stress and strain of ice-rich frozen silt with various temperatures and initial water contents, and the meso-damage evolution of an ice-rich frozen silt specimen during the loading process was recorded. They found that the effect of temperature on the initial elastic modulus of ice-rich frozen silt was not obvious, and the initial density damage of each layer of specimens showed nonuniformity. Ma et al. [13] conducted pressuremeter tests on ice-rich permafrost with relatively high temperature at the railway embankment site and found that the sensitivities of shear modulus of frozen clay with larger ice contents to environment temperature were higher than those of original frozen soil. Zhang et al. [14] performed static triaxial compressive tests on frozen silty sand with large-scale volumetric ice contents (24% to 99.5%); test results illustrated that at relatively low volumetric ice content, the static curve characteristics of specimens gradually changed from strain softening to strain hardening with increasing confining pressure. However, for specimens with high volumetric ice content (75% to 99.5%), the curves showed strain softening characteristic within the test confining pressure range (0.05 MPa to 4 MPa). Moreover, the static triaxial compressive strength of ice-rich silty sand specimens decreased monotonically with the increase in volumetric ice content until 60%, after which the strength increased.

The above experimental researches are mainly concentrated on the static mechanical response of ice-rich frozen soil, but in shortage of the strength and energy dissipation characteristic of ice-rich frozen soil in the high loading rate range. The frozen soil dynamics has gradually become one of the front-burner research issues, and it mainly involves frozen soil blasting, drilling, and impact engineering fields [15]. Additionally, the energy dissipation is identified as the driving force of the crack initiation, propagation, accumulation, and penetration of frozen soil materials, and its process is irreversible under impact loads [16]. Therefore, analysis of the dynamic energy dissipation characteristic, mainly including energy absorption rate and reflectance, can facilitate realizing the dynamic damage process of ice-rich frozen soil. The split Hopkinson pressure bar (SHPB) system has been extensively acknowledged to test the dynamic properties and energy dissipation characteristics of various engineering materials, such as frozen soil [17], rock [18], concrete [19], and coal [20]. Many valuable conclusions have been obtained; for example, by conducting dynamic compressive tests on granite with the help of an SHPB device, the absorption energy density of specimens were found to have a linear correlation with the strain rate; moreover, the fractal dimension was an effective index to assess the dynamic energy dissipation behavior of rock specimens [21]. Zhang et al. [22] analyzed the energy dissipation parameters for coal materials in SHPB tests and found that the transmission energy and dissipation energy density of coal specimens under impact load are much lower than those of rock. Xiong et al. [23] investigated the energy dissipation characteristic of loess specimens with various strain rates and dry densities under passive confining pressure state, and test results demonstrated that the friction force between soil particles became larger at higher initial density, resulting in the increase in absorbed energy for reaching the destruction state. Ma et al. [24] observed that both the confining pressure and loading pressures showed positive effect on the values of absorbed energy.

It is highly worthwhile to understand the energy dissipation process of ice-rich frozen soil under dynamic loads for promoting the blasting efficiency of frozen soil and the design of underground explosion-proof structure. In the present work, frozen sandy soil specimens with six initial water contents were prepared at first, and the dynamic compression tests were conducted on frozen sandy soil using an aluminum SHPB system with 37 mm diameter. Finally, the sensitivities of strain rate, water content, and temperature on energy parameters and energy dissipation parameters were systematically analyzed.

2. Frozen Soil Preparation and Energy Calculation

2.1. Frozen Soil Preparation with Various Water Contents. The particle size of the disturbed sandy soil is shown in Table 1. After the processes of drying, rolling, screening, and mixing for the undisturbed soil, the remolded sandy soil specimens are obtained to reduce the discreteness of test data. One of the objectives is to analyze the energy dissipation parameters of frozen soil with various water contents. Therefore, frozen sandy specimens with original state (15%) to 110% water content are prepared. However, it is a crucial technical problem to prepare homogeneous frozen soil specimens with high water content. In this test, the ice-soil-water mixing method proposed by the previous investigation is adopted to prepare the frozen sandy soil specimens with water contents from 45% to 110% [25], while the conventional soil preparation method is used to make specimens with other water contents. The specimen size for dynamic tests is $\Phi 37\,\text{mm} \times 18.5\,\text{mm}$, as shown in Figure 1. After the unfrozen specimens were

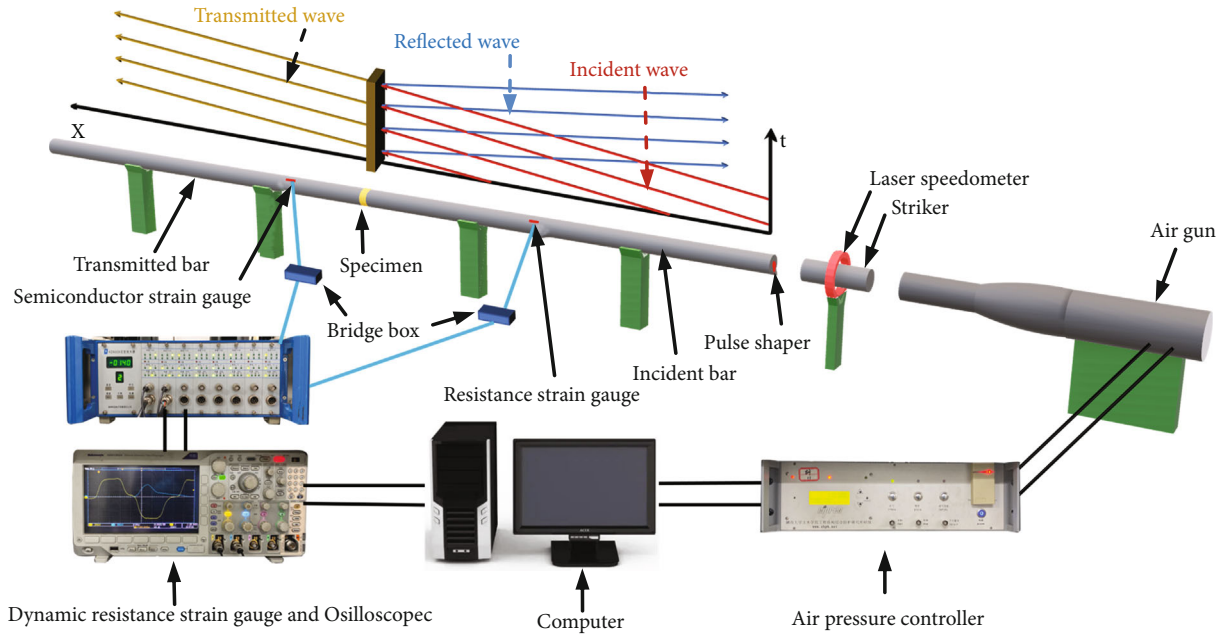

Figure 2: SHPB device.

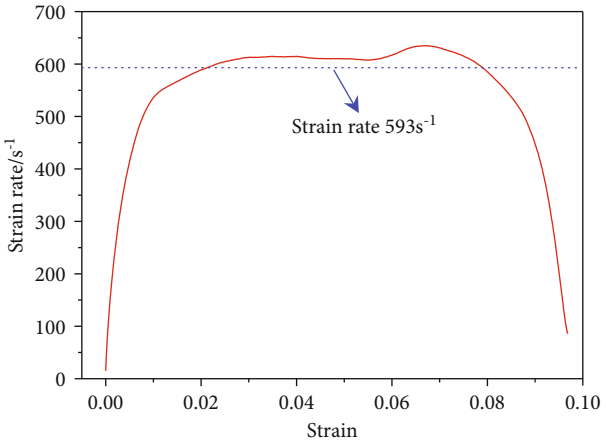

Figure 3: The typical strain rate time history curve.

prepared well, they are put in a low cryogenic box at the designed temperatures (i.e., -5°C, -10°C, and -15°C) until testing.

2.2. SHPB System and Energy Calculation. This research uses the SHPB system to obtain the dynamic energy parameters of frozen soil, which has been widely employed in frozen soil dynamic tests. As shown in Figure 2, the high-pressure air gun can achieve the striker bar to impact the incident bar with various speeds. Strain gauge sensors are pasted on the incident and transmission bars to collect strain signals, respectively. The striker, incident, and transmission bars are made of aluminum materials with 37 mm diameter, and their elastic modulus E and longitudinal wave velocity C are 70 GPa and 5090 m/s, respectively. In order to obtain a longer rise time of incident wave, a waveform shaper is used and mounted on the front of the incident bar [26]. All the are collected by using the oscilloscope.

Figure 3 shows the typical strain rate time history curve, it can be observed that there exists an approximate constant strain rate platform in the curves, indicating that the SHPB test can achieve constant strain rate loading, and the experimental data are valid [27].

The calculation principles of incident energy $E_I(t)$, reflected energy $E_R(t)$, and transmitted energy $E_T(t)$ are as follows [28]:

$$E_I(t) = \mathrm{EAC}\int_0^t \varepsilon_I^2(t)dt, \tag{1}$$

$$E_R(t) = \mathrm{EAC}\int_0^t \varepsilon_R^2(t)dt, \tag{2}$$

$$E_T(t) = \mathrm{EAC}\int_0^t \varepsilon_T^2(t)dt, \tag{3}$$

where $\varepsilon(t)$ and t are the strain and time of stress waves, respectively, and A is the cross-sectional area of bars.

In general, the absorption energy of the test specimen is obtained by subtracting three wave energies; however, for frozen soil materials with relatively small wave impedance, Ma et al. [29] have proposed a calculation formula to obtain the absorption energy of frozen soil $E_S(t)$ based on stress balance theory:

$$E_S(t) = -\mathrm{EAC}\int_0^t 2\varepsilon_T\varepsilon_R dt. \tag{4}$$

In addition to the absorption energy and reflected energy, the absorption energy rate η_s is also calculated to describe the energy utilization efficiency, as shown in the

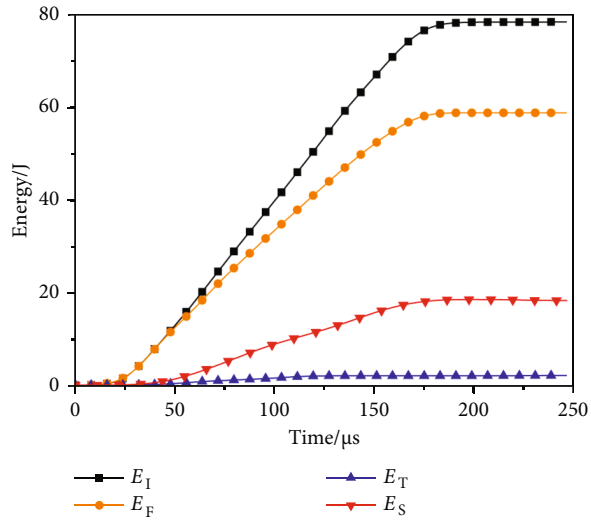

Figure 4: The typical energy-time curve of frozen sandy soil.

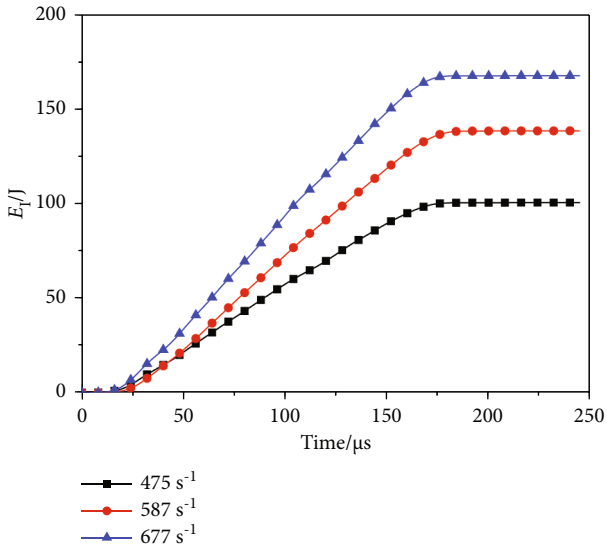

Figure 5: The incident energy curves with various strain rates.

following [30]:

$$\eta_s = \frac{E_S}{E_I} \times 100\%. \quad (5)$$

2.3. Test Design and Research Significance. The objective of this study is to explore the dynamic energy dissipation characteristics of frozen soil under different conditions. Therefore, these considerations of strain rate, water content, and temperature are chosen as the factors which may significantly affect the energy dissipation characteristics of frozen sandy soil. In this test, six water contents (i.e., 15%, 25%, 37.5%, 45%, 80%, and 110%) are designed for preparing the sandy soil specimens, and these specimens are placed in three low temperatures (i.e., -5°C, -10°C, and -15°C). Finally, three impact pressures (i.e., 0.2 MPa, 0.3 MPa, 0.35 MPa) are conducted in the SHPB test to achieve various strain rates of specimens.

3. Analysis of Energy Dissipation Characteristic

3.1. Energy-Time Curves. Figure 4 presents the typical energy-time curve of frozen sandy soil under dynamic loads. As the loading time increases, the incident energy, reflected energy, absorption energy, and transmitted energy linearly increase to a constant value. It can be also noticed that the sum of absorption and transmitted energies accounts for low proportion of the incident energy, and most of the energy derived from the incident wave is reflected. The above phenomenon arises from the low wave impedance characteristic of frozen soil material, which is not conducive to stress wave propagation [31]. It is commonly accepted that the destruction of specimens is attributed to the incident energy, and its values are mainly affected by the strain rate. Therefore, the variation in the incident energy with strain rate is analyzed. Figure 5 presents the incident energy curves with various strain rates. Both the rise rate and final value of incident energy E_I gradually increase with the increasing strain rate.

3.2. Energy Parameters of Frozen Soil. In this research, the influences of strain rate, water content, and temperature on the absorption energy, reflected energy, and absorption energy rate are studied in detail. Figure 6 presents the variation in absorption energy and reflected energy with strain rate at -5°C. Both the absorption energy and reflected energy are closely related to strain rate, exhibiting a positive correlation. Figure 6(a) illustrates that the absorption energy of frozen sandy soil decreases monotonically with the increase in water content, and the strain rate-dependent effect of absorption energy is more obvious at low water content scope (15% to 37.5%) compared with that at high water contents (45% to 110%). Moreover, Figure 6(b) reveals that the water content shows no significant effect on the reflected energy. The average value of reflected energy E_R is 161 J at 700 s^{-1}, which is much higher than the value of 72 J at 475 s^{-1}, with a large-scale increase of 123.6%. Compared with the soil particles, both the ice particles and the bonding surface require lower energy to reach the failure state. Therefore, the proportion of ice particles inside the specimen gradually increases with the increasing water content, resulting in the decrease in the absorption energy.

In addition to the absorption energy and reflected energy, the value of absorption energy rate represents the energy absorption efficiency. Hence, the analysis of the effects of test parameters on absorption energy rate was performed in this work. The absorption energy rates of frozen sandy soil with various conditions are shown in Figure 7.

As shown in Figure 7(a), in the range of 400 s^{-1} to 700 s^{-1}, the strain rate presents small influence on the values of absorption energy rate. For frozen sandy soil specimens with 45% to 110% contents, the values of absorption energy rate is in the range of 5% to 7%, and it is between 11% and 14.3% for the specimens with 15% to 37.5% water contents. Therefore, the absorption energy rates of specimens

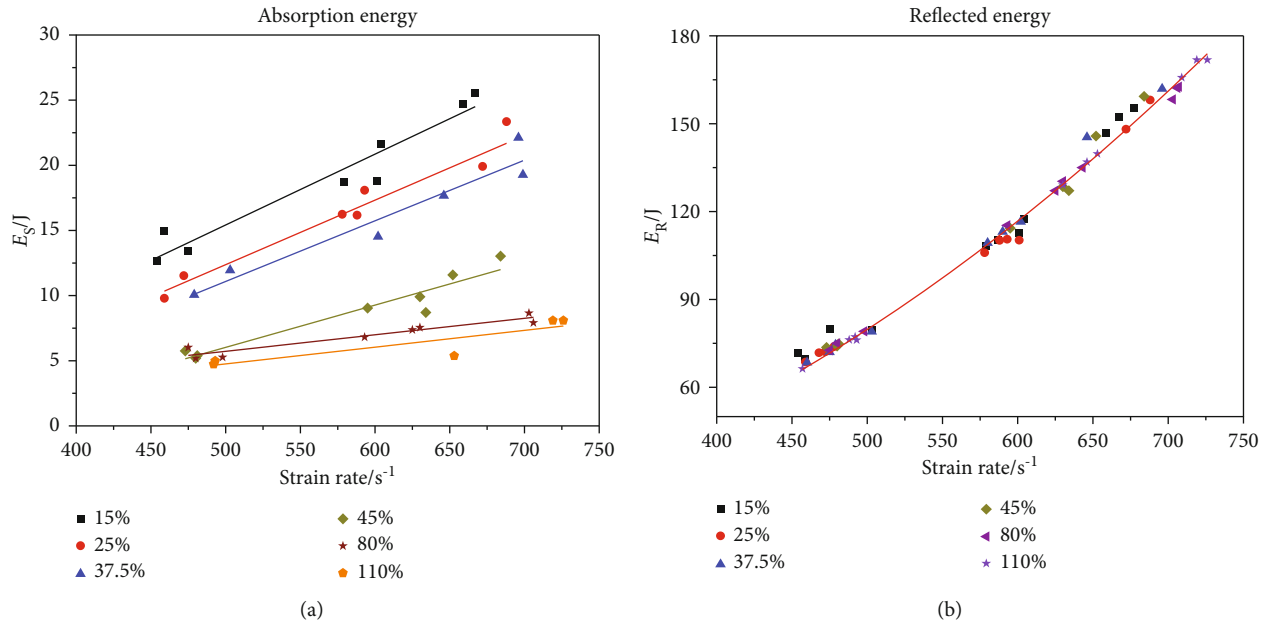

Figure 6: The variation in absorption energy and reflected energy with strain rate.

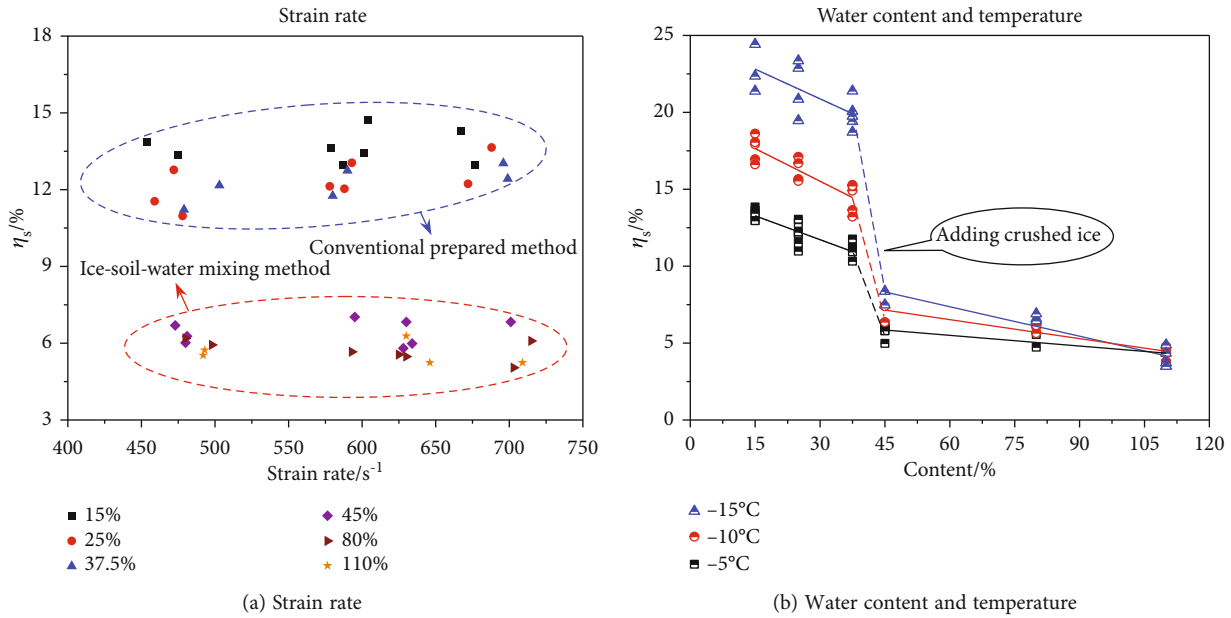

Figure 7: The absorption energy rate of frozen sandy soil with various conditions.

prepared by the conventional method are much higher compared with those by the ice-soil-water mixing method. Figure 7(b) demonstrates that with the increase in water content, a continuous decreasing regular is observed for the value of absorption energy rate. Moreover, the decreasing rate exhibits "fast-rapid-slow" characteristic, and the turn points appear at 37.5% and 45%, respectively. For instance, at -10°C, the average absorption energy rate decreases from 17.6% to 14.5% when the water content increases from 15% to 37.5%, with a reduction of 18%. However, it substantially decreases to 6.9% at 45% water content, with a large-scale reduction of 61% compared with that at 15% water content. Moreover, the absorption energy rate increases with the decreasing temperature under the same water contents, indicating that the low temperature contributes to the improvement of energy absorption efficiency. This phenomenon also has been found and reported in the aforementioned investigation [24].

3.3. Energy Dissipation Characteristic under Different Stages. Under dynamic loads, the stress wave amplitude is varying for frozen soil at different positions, which results in a large deformation degree of frozen soil material. From the dynamic stress-strain curves, it can be noticed that the

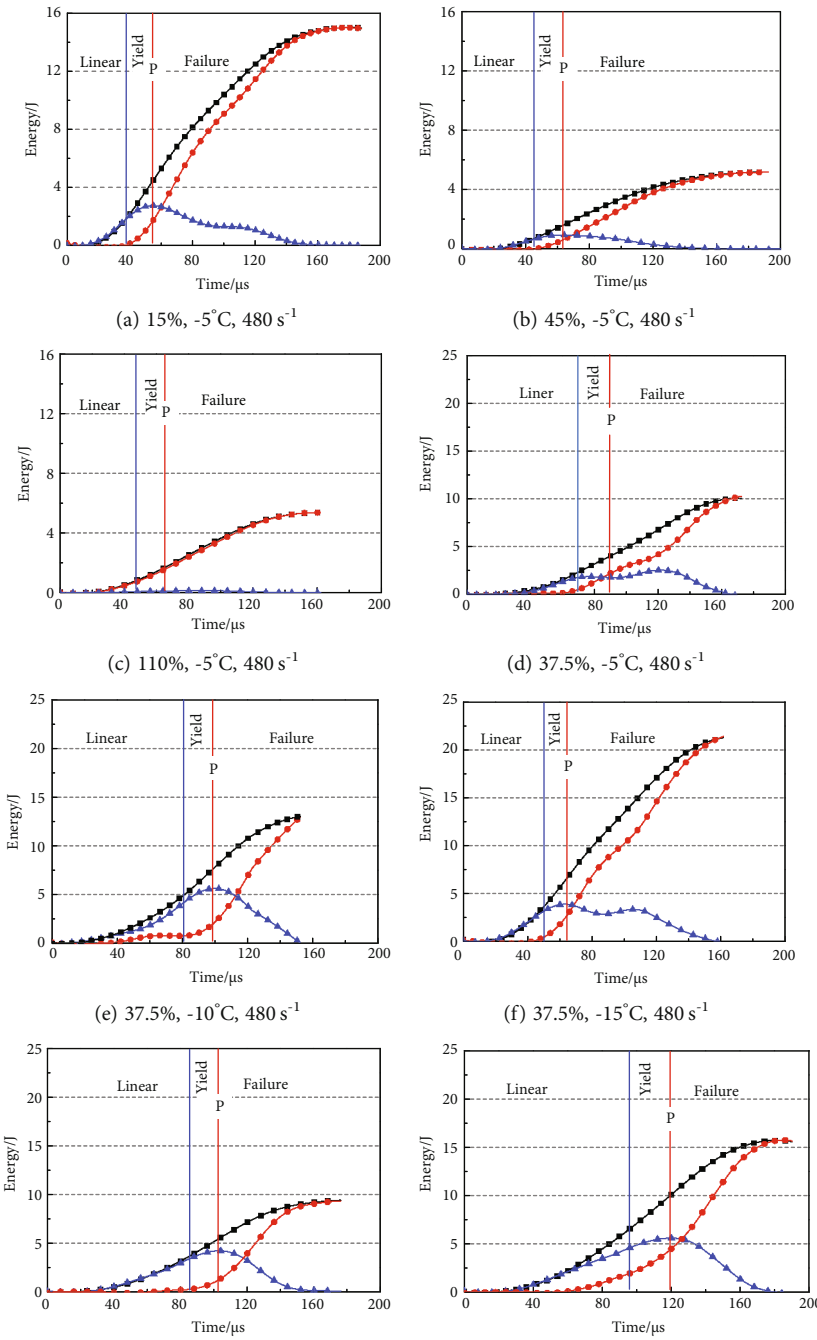

(a) 15%, -5°C, 480 s^{-1}

(b) 45%, -5°C, 480 s^{-1}

(c) 110%, -5°C, 480 s^{-1}

(d) 37.5%, -5°C, 480 s^{-1}

(e) 37.5%, -10°C, 480 s^{-1}

(f) 37.5%, -15°C, 480 s^{-1}

(g) 25%, -5°C, 478 s^{-1}

(h) 25%, -5°C, 601 s^{-1}

Figure 8: Continued.

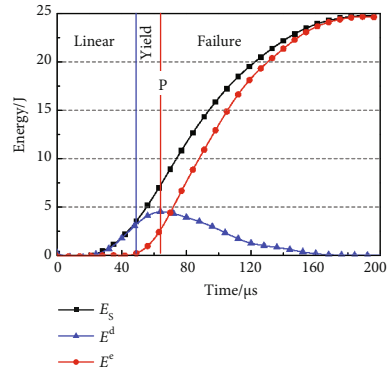

(i) 25%, -5°C, 659 s^{-1}

FIGURE 8: The energy dissipation characteristic under different deformation stages.

deformation of frozen soil can be approximately divided into three stages: elastic, plastic, and failure stages. Therefore, the energy dissipation characteristics of frozen sandy soil with various stages are systematically analyzed. The energy absorbed by the specimen is mainly consumed in the following two forms: (1) elastic strain energy stored inside the specimen (releasable elastic strain energy E^e) and (2) the propagation of micro- and macrocracks (dissipation energy E^d). By equation (4), the absorption energy during the loading process can be calculated. In addition, the values of E^e and E^d can be expressed as [32]

$$E^e = \frac{1}{2}\sigma\varepsilon^e = \frac{\sigma}{2E}, \tag{6}$$

$$E^d = E_S - E^e, \tag{7}$$

where E and σ are the deformation modulus and stress of frozen sandy soil, respectively.

According to the above equations, the absorption energy E_s, releasable elastic strain energy E^e, and dissipation energy E^d of frozen sandy soil with various deformation stages are obtained and shown in Figure 8. It can be observed that the energy dissipation parameters are closely associated with the water content, temperature, and strain rate. In addition, different energy dissipation characteristics are found during the loading process; specifically, at the linear stage, the frozen soil specimens exhibit mainly elastic deformation; both the absorption energy E_s and releasable elastic strain energy E^e show a synchronous upward trend, and the proportion of dissipated energy E^d is negligible. At the yield stage, the plastic deformation ratio of the specimen increases; therefore, the increased speed of releasable elastic strain energy E^e decreases; as a comparison, the dissipated energy E^d begins to increase rapidly. Finally, after reaching the peak strength, the internal damage of frozen soil increases gradually, and the microcracks inside the specimen rapidly spread and coalesce and gradually evolve into macrocracks. Therefore, the releasable elastic strain energy E^e continues decreasing until 0; the dissipated energy E^d accounts for the main ratio of the absorption energy E_s.

4. Conclusions

In the present study, SHPB compression tests were conducted on an ice-rich frozen soil specimen to investigate the water content dependency of dynamic energy dissipation characteristic. Furthermore, the proportions of absorption energy, releasable elastic strain energy, and dissipation energy during dynamic deformation were analyzed. The following conclusions could be drawn:

(1) In SHPB tests, the incident energy E_I, reflected energy E_R, absorption energy E_S, and transmitted energy E_T linearly increase to a constant value with the deformation of the specimen. Both the absorption energy E_S and transmitted energy E_T account for the low proportion of the total incident energy E_I, while most of the energy is reflected

(2) The strain rate shows positive effects on the absorption energy E_S and reflected energy E_R. However, the water content shows no significant effect on the reflected energy E_R. When the water content increases from 15% to 110%, the absorption energy rate gradually decreases, and the decreasing rate exhibits "fast-rapid-slow" characteristic, and the turn points appear at 37.5% and 45%, respectively

(3) At the linear stage, both the absorption energy E_S and releasable elastic strain energy E^e show a synchronous upward trend, and the proportion of dissipated energy E^d is negligible. At the yield stage, the increased speed of releasable elastic strain energy E^e decreases, while the dissipated energy E^d begins to increase rapidly. After reaching the peak strength, the releasable elastic strain energy E^e continues decreasing until 0; the dissipated energy E^d accounts for the main ratio of the absorption energy E_S

Data Availability

The datasets in this study are available from the corresponding author on reasonable request.

Conflicts of Interest

The authors declare that there are no conflicts of interest regarding the publication of this paper.

Acknowledgments

This study was supported by the Opening Foundation of the State Key Laboratory of Frozen Soil Engineering (No. SKLFSE202004), Anhui Provincial Natural Science Foundation (No. 1908085QE212), China Postdoctoral Science Foundation (No. 2019M652162), Doctoral Fund Project of Anhui University of Science & Technology (No. 11695), and Graduate Innovation Foundation of Anhui University of Science & Technology (2021CX2037).

References

[1] D. Wang, E. L. Liu, D. Zhang et al., "An elasto-plastic constitutive model for frozen soil subjected to cyclic loading," *Cold Regions Science and Technology*, vol. 189, article 103341, 2021.

[2] Z. Y. Yan, W. Pan, J. J. Feng, and Z. H. Liu, "Numerical simulation of thawing process in frozen soil," *Geofluids*, vol. 2020, Article ID 8822320, 7 pages, 2020.

[3] A. A. Aldaeef and M. T. Rayhani, "Pile-soil interface characteristics in ice-poor frozen ground under varying exposure temperature," *Cold Regions Science and Technology*, vol. 191, article 103377, 2021.

[4] K. P. Lijith, V. Sharma, and D. N. Singh, "Shear strength characteristics of frozen fine sands under direct shear testing conditions," *International Journal of Geomechanics*, vol. 22, no. 2, p. 04021268, 2022.

[5] L. Y. Zhao, Y. M. Lai, J. F. Shao, W. L. Zhang, Q. Z. Zhu, and F. J. Niu, "Friction-damage coupled models and macroscopic strength criteria for ice- saturated frozen silt with crack asperity variation by a micromechanical approach," *Engineering Geology*, vol. 294, article 106405, 2021.

[6] N. Girgis, B. Li, S. Akhtar, and B. Courcelles, "Experimental study of rate-dependent uniaxial compressive behaviors of two artificial frozen sandy clay soils," *Cold Regions Science and Technology*, vol. 180, article 103166, 2020.

[7] W. Ma and D. Y. Wang, "Studies on frozen soil mechanics in China in past 50 years and their prospect," *Chinese Journal of Geotechnical Engineering*, vol. 34, no. 4, pp. 625–640, 2012.

[8] Y. M. Lai, Y. Zhang, S. J. Zhang, L. Jin, and X. X. Chang, "Experimental study of strength of frozen sandy soil under different water contents and temperatures," *Rock and Soil Mechanics*, vol. 30, no. 12, pp. 3665–3670, 2009.

[9] H. Zhang, J. M. Zhang, K. Su, and S. W. Liu, "In-site pressuremeter creep test on high-temperature and high ice-rich permafrost," *Journal of Jilin University(Earth Science Edition)*, vol. 43, no. 6, pp. 1950–1957, 2013.

[10] G. S. Yang, B. Bai, and X. L. Yao, "Study of thawing and consolidation law of ice-rich embankment," *Rock and Soil Mechanics*, vol. 41, no. 3, pp. 1010–1018, 2020.

[11] M. T. Cai, J. M. Zhang, W. Ma, Z. H. Yin, Y. H. Mu, and H. Zhang, "Thermal influences of stabilization on warm and ice-rich permafrost with cement: field observation and numerical simulation," *Applied Thermal Engineering*, vol. 148, pp. 536–543, 2019.

[12] Y. G. Yang, Y. M. Lai, Y. B. Pu, and Q. B. Li, "Experimental analysis of damage of ice-rich frozen silt under uniaxial compression," *Rock and Soil Mechanics*, vol. 31, no. 10, pp. 3063–3068, 2010.

[13] X. J. Ma, J. M. Zhang, B. Zheng, and S. Y. Li, "Study on warm and ice-rich permafrost beneath Qinghai-Tibet railway embankment with pressiometer," *Rock and Soil Mechanics*, vol. 29, no. 3, pp. 764–768, 2008.

[14] S. J. Zhang, H. M. Du, and J. Harbor, "The effect of confining pressure and water content on compressive strength and deformation of ice-rich silty sand," *Permafrost and Periglac. Process*, vol. 28, no. 1, pp. 298–305, 2017.

[15] D. D. Ma, H. S. Xiang, Q. Y. Ma et al., "Dynamic damage constitutive model of frozen silty soil with prefabricated crack under uniaxial load," *Journal of Engineering Mechanics*, vol. 147, no. 6, article 04021033, 2021.

[16] B. X. Wang, Y. B. Wang, C. X. Fan, and W. D. Zhang, "Energy distribution and evolution of frozen silty clay at subzero temperatures under compressive loading," *Transportation Geotechnics*, vol. 31, article 100656, 2021.

[17] Q. Y. Ma, K. Huang, and D. D. Ma, "Energy absorption characteristics and theoretical analysis of frozen clay with pre-existing cracks under uniaxial compressive impact load," *Cold Regions Science and Technology*, vol. 182, article 103206, 2021.

[18] H. W. Ren, D. S. Zhang, S. X. Gong et al., "Dynamic impact experiment and response characteristics analysis for 1:2 reduced-scale model of hydraulic support," *International Journal of Mining Science and Technology*, vol. 31, no. 3, pp. 347–356, 2021.

[19] X. Chen, X. Z. Shi, J. Zhou, E. M. Li, P. Y. Qiu, and Y. G. Gou, "High strain rate compressive strength behavior of cemented paste backfill using split Hopkinson pressure bar," *International Journal of Mining Science and Technology*, vol. 31, no. 3, pp. 387–399, 2021.

[20] X. J. Hao, W. S. Du, Y. X. Zhao et al., "Dynamic tensile behaviour and crack propagation of coal under coupled static-dynamic loading," *International Journal of Mining Science and Technology*, vol. 30, no. 5, pp. 659–668, 2020.

[21] F. Q. Gong, H. Y. Jia, Z. X. Zhang, J. Hu, and S. Luo, "Energy dissipation and particle size distribution of granite under different incident energies in SHPB compression tests," *Shock and Vibration*, vol. 2020, Article ID 8899355, 14 pages, 2020.

[22] W. Q. Zhang, B. M. Shi, and C. M. Mu, "Experimental research on failure and energy dissipation law of coal under impact load," *Journal of Mining & Safety Engineering*, vol. 33, no. 2, pp. 375–380, 2016.

[23] Z. M. Xiong, S. H. Lu, Y. L. Li et al., "Research on dynamic properties and energy dissipation of loess under passive confining pressure conditions," *Rock and Soil Mechanics*, vol. 42, no. 3, pp. 775–782, 2021.

[24] Q. Y. Ma, D. D. Ma, P. Yuan, and Z. M. Yao, "Energy absorption characteristics of frozen soil based on SHPB test," *Advances in Materials Science and Engineering*, vol. 2018, Article ID 5378173, 9 pages, 2018.

[25] S. J. Zhang, W. Ma, Z. Z. Sun, and H. M. Du, "Analysis and discussion of different methods of artificial ice-high specimen preparation," *Sciences in Cold and Arid Regions*, vol. 6, no. 5, pp. 0440–0446, 2014.

[26] F. L. Zhang, Z. W. Zhu, W. Ma, Z. W. Zhou, and T. T. Fu, "A unified viscoplastic model and strain rate-temperature

equivalence of frozen soil under impact loading," *Journal of the Mechanics and Physics of Solids*, vol. 152, article 104413, 2021.

[27] D. D. Ma, Q. Y. Ma, P. Yuan, and Z. M. Yao, "SHPB tests on artificial frozen sand and its analysis under active confining pressure," *Rock and Soil Mechanics*, vol. 38, no. 10, pp. 2957–2961, 2017.

[28] M. Chen, H. Q. Si, X. C. Fan, Y. W. Xuan, and M. Z. Zhang, "Dynamic compressive behaviour of recycled tyre steel fibre reinforced concrete," *Construction and Building Materials*, vol. 316, article 125896, 2022.

[29] D. D. Ma, Q. Y. Ma, Z. M. Yao, and K. Huang, "Static-dynamic coupling mechanical properties and constitutive model of artificial frozen silty clay under triaxial compression," *Cold Regions Science and Technology*, vol. 167, article 102858, 2019.

[30] B. Cao, S. Yoshida, T. Iwamoto, and H. T. Pham, "Development of impact small punch test for investigating energy absorption," *International Journal of Mechanical Sciences*, vol. 208, article 106675, 2021.

[31] Q. Li, W. L. Shu, L. Cao, W. W. Duan, and B. Zhou, "Vertical vibration of a single pile embedded in a frozen saturated soil layer," *Soil Dynamics and Earthquake Engineering*, vol. 122, pp. 185–195, 2019.

[32] P. Wang, J. Y. Xu, X. Y. Fang, and P. X. Wang, "Energy dissipation and damage evolution analyses for the dynamic compression failure process of red-sandstone after freeze-thaw cycles," *Engineering Geology*, vol. 221, pp. 104–113, 2017.